

Supplementary Information: Transition between [R]- and [S]-Stereoisomers without Bond Breaking

Shampa Raghunathan,[†] Komal Yadav,[‡] V. C. Rojisha,[†] Tanashree Jaganade,[†] V.
Prathyusha,[†] Swetha Bikkina,[†] U. Lourderaj,^{*,‡} and U. Deva Priyakumar^{*,†}

[†]*Center for Computational Natural Sciences and Bioinformatics International Institute of
Information Technology, Hyderabad 500 032, India*

[‡]*School of Chemical Sciences, National Institute of Science Education and Research,
Bhubaneswar, India*

E-mail: u.lourderaj@niser.ac.in; deva@iiit.ac.in

1. Methods

EDA-NOCV analysis The nature of interactions between the C_2H_4X fragment and in p-X and t-X ($X = Si, Al^-$ and P^+) were analyzed by energy decomposition analysis combined with natural orbitals for chemical valence (EDA-NOCV) analysis.^[1] EDA-NOCV analysis is performed at the BP86 level of theory with a triple- ζ basis set having two sets of polarization functions with a frozen-core approximation for the core electrons (BP86/TZ2P)^[2] using ADF 2016.107 program.^[3-5]

Ab initio classical trajectory simulations Additional set of 30 trajectories for each system were calculated, which initiated in the reactant region with higher total energies of 52.28, 48.65, and 46.60 kcal/mol for Si, Al^- , and P^+ systems, respectively. The number of reactive trajectories following the racemization and the ring opening paths are given in Table S1.

Table S1: Details of trajectories showing stereomutation initiated with higher total energies.

| Systems | Energy (kcal/mol) | No. of trajectories showing stereomutation | No. of trajectories showing ring opening path |
|------------------|-------------------|--|---|
| $[Si(C_4)H_4]$ | 48.65 | 10 | 1 |
| $[Al(C_4)H_4]^-$ | 52.28 | 20 | 0 |
| $[P(C_4)H_4]^+$ | 46.60 | 2 | 15 |

2. Results of electronic structure calculations

2.1 Energies

Table S2: Relative energies of transition states/intermediates (in kcal mol⁻¹) obtained at the MP2 and CCSD(T) levels of theory using the cc-pVTZ basis set. Transition state, c[‡]-P corresponds to the closed-planar to closed-tetrahedral transition and r[‡]-X corresponds to the ring opening transition state.

| Species | MP2 | CCSD(T) ^a |
|---|-------|----------------------|
| [Si(C₄)H₄] | | |
| p-Si | 4.76 | 4.51 |
| t-Si | 0.00 | 0.00 |
| r [‡] -Si | 11.34 | 8.53 |
| r-Si | 11.26 | 8.56 |
| [Al(C₄)H₄]⁻ | | |
| p-Al | 3.66 | 3.52 |
| t-Al | 0.00 | 0.00 |
| r [‡] -Al | 8.99 | 7.83 |
| r-Al | 8.37 | 7.44 |
| [P(C₄)H₄]⁺ | | |
| p-P | 5.19 | 4.49 |
| c [‡] -P | 5.63 | 4.30 |
| t-P | 0.00 | 0.00 |
| r [‡] -P | 5.62 | 3.80 |
| r-P | 5.44 | 1.20 |

^a Values given from single point energy calculations at CCSD(T) level using the MP2 optimized geometries.

It can be seen from Tables S3 and S4 that, for **p-Si**, the MP2/cc-pVTZ level of theory gives lower energy than the CASSCF(8,8) and CASSCF(14,14) methods. Including static correlation using (8,8) active space increases the **r[‡]-Si** energy. While for **r[‡]-Si**, the MP2 energy is higher than that obtained using CASSCF methods. It should be pointed that for both **p-Si** and **r[‡]-Si** the largest deviation of MP2 energies from the CASSCF and CASPT2 values is only about 3 kcal/mol. In the case of X = P system, a similar trend was observed with MP2 energies lower than the CASSCF energies and with even smaller deviations in energies. Thus, for the ab initio dynamical simulations, the MP2/cc-pVTZ level of theory was considered.

Table S3: Relative single point energies (in kcal mol⁻¹) on MP2/cc-pVTZ optimized geometries at CASSCF(8,8)/cc-pVTZ and CASPT2(8,8)/cc-pVTZ level of theories. Transition state, r[‡]-X corresponds to the ring opening transition state.

| Species | MP2 | CASSCF | CASPT2 |
|---|------|--------|--------|
| [Si(C₄)H₄] | | | |
| p-Si | 4.8 | 5.6 | 6.8 |
| t-Si | 0.0 | 0.0 | 0.0 |
| r [‡] -Si | 11.3 | 8.0 | 10.7 |

Table S4: Relative single point energies (in kcal mol⁻¹) on MP2/cc-pVTZ optimized geometries at CASSCF(14,14)/cc-pVTZ level of theory. Transition state, c[‡]-P corresponds to the closed-planar to closed-tetrahedral transition and r[‡]-X corresponds to the ring opening transition state.

| Species | MP2 | CASSCF |
|--|------|--------|
| [Si(C₄)H₄] | | |
| p-Si | 4.8 | 6.1 |
| t-Si | 0.0 | 0.0 |
| r [‡] -Si | 11.3 | 7.9 |
| [P(C₄)H₄]⁺ | | |
| p-P | 5.2 | 7.0 |
| c [‡] -P | 5.6 | 6.1 |
| t-P | 0.0 | 0.0 |
| r [‡] -P | 5.6 | 5.3 |

2.2 Structures

| Intermediates of $[\text{Si}(\text{C}_4)\text{H}_4]$ | | |
|--|---|--|
| | | |
| p-Si $\theta = 69.4^\circ$ $\phi = 0.0^\circ$ $N_{imag} = 1(102.4i)$ | t-Si $\theta = 69.4^\circ$ $\phi = 90.0^\circ$ $N_{imag} = 0$ | r-Si $\theta = 180.0^\circ$ $\phi = 0.0^\circ$ $N_{imag} = 0$ |
| Intermediates of $[\text{Al}(\text{C}_4)\text{H}_4]^-$ | | |
| | | |
| p-Al $\theta = 71.1^\circ$ $\phi = 0.0^\circ$ $N_{imag} = 1(134.5i)$ | t-Al $\theta = 71.1^\circ$ $\phi = 90.0^\circ$ $N_{imag} = 0$ | r-Al $\theta = 180.0^\circ$ $\phi = 0.0^\circ$ $N_{imag} = 0$ |
| Intermediates of $[\text{P}(\text{C}_4)\text{H}_4]^+$ | | |
| | | |
| p-P $\theta = 67.8^\circ$ $\phi = 0.0^\circ$ $N_{imag} = 0$ | t-P $\theta = 68.1^\circ$ $\phi = 90.0^\circ$ $N_{imag} = 0$ | r-P $\theta = 109.2^\circ$ $\phi = 96.4^\circ$ $N_{imag} = 0$ |
| Transition states | | |
| | | |
| r^\ddagger-Si $\theta = 154.3^\circ$ $\phi = 116.7^\circ$ $N_{imag} = 1(71.8i)$ | r^\ddagger-Al $\theta = 137.6^\circ$ $\phi = 103.7^\circ$ $N_{imag} = 1(110.6i)$ | r^\ddagger-P $\theta = 92.8^\circ$ $\phi = 91.8^\circ$ $N_{imag} = 1(150.8i)$ |

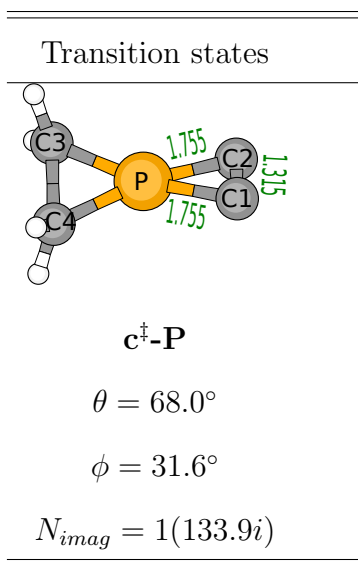


Figure S1: Optimized structures and selected geometrical parameters of planar (p-X), tetrahedral (t-X), ring-opened (r-X) minima, and transition state ($\mathbf{r^{\ddagger}\text{-X}}$) of $\text{X}(\text{C})_4\text{H}_4$ systems at MP2/cc-pVTZ level of theory; in case of $\text{X}=\text{P}^+$, the transition state ($\mathbf{c^{\ddagger}\text{-P}}$) responsible for planar to tetrahedral transition. Bond distances (in Å), angle between two three-membered rings (ϕ , degree), $\angle\text{X-C1-C2}$ (θ , degree), and N_{imag} representing number of imaginary frequency with values given in parentheses.

Bonding analysis using EDA-NOCV method In order to get a quantitative interpretation of chemical bonds to assess the stability of the planar versus tetrahedral $\text{X}(\text{C})_4\text{H}_4$ systems we have performed the EDA-NOCV analysis. To this end, the instantaneous interaction energy ΔE_{int} was computed between two fragments $\text{C}\equiv\text{C}$ and XC_2H_4 units (See Figure S2(a) for the scheme). The total interaction energy ΔE_{int} is decomposed as,

$$\Delta E_{int} = \Delta E_{Pauli} + \Delta E_{elstat} + \Delta E_{orb} \quad . \quad (1)$$

Where 1st, 2nd and 3rd terms refer to Pauli repulsion, electrostatic and orbital interaction energies, respectively; further the bond dissociation energy (by definition with opposite sign) $-D_e = (\Delta E_{int} + \Delta E_{prep})$.^[1] Here ΔE_{prep} refers to preparation energy. The best bonding situation for p-X and t-X systems inferred from these analyses are depicted in Figure S2(b), and results are given in Table S5. The EDA-NOCV results indicate that the nature of interaction of the $\text{C}\equiv\text{C}$ fragment with the remaining one varies from planar to tetrahedral compounds.

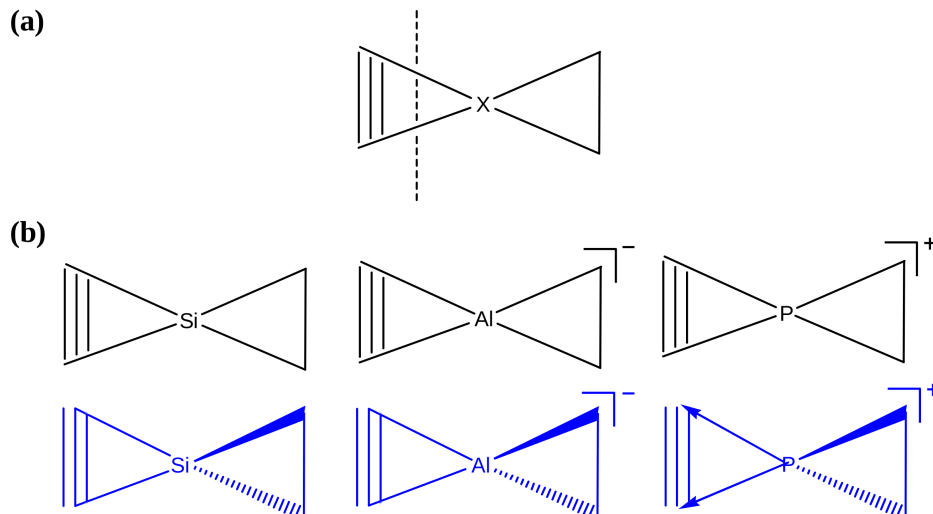


Figure S2: (a) Fragmentation scheme used for EDA-NOCV analyses. (b) Best bonding representation for p-X and t-X from EDA-NOCV analyses.

Table S5: Energy decomposition analyses (values in kcal/mol) of p-X and t-X systems at BP86/TZ2P. X=C was considered as well for comparison.

| | ΔE_{int} | ${}^a\Delta E_{Pauli}$ | ${}^a\Delta E_{elstat}$ | ΔE_{orb} | ΔE_{prep} | D_e |
|------|------------------|------------------------|-------------------------|------------------|-------------------|--------|
| p-C | -173.7 | 434.9 | -213.2 | -395.4 | 41.4 | -132.3 |
| | | | (35.0%) | (65.0%) | | |
| t-C | -314.0 | 642.2 | -332.8 | -623.4 | 221.5 | -92.5 |
| | | | (34.8%) | (65.2%) | | |
| p-Si | -174.8 | 264.5 | -129.9 | -309.4 | 64.7 | -110.1 |
| | | | (29.6%) | (70.4%) | | |
| t-Si | -247.3 | 267.6 | -132.7 | -382.2 | 135.1 | -112.3 |
| | | | (25.8%) | (74.2%) | | |
| p-Al | -206.6 | 208.2 | -116.4 | -298.4 | 56.8 | -149.8 |
| | | | (28.1%) | (71.9%) | | |
| t-Al | -232.4 | 214.6 | -117.7 | -329.3 | 80.4 | -152.0 |
| | | | (26.3%) | (73.7%) | | |
| p-P | -134.5 | 326.5 | -118.7 | -342.4 | 53.4 | -81.1 |
| | | | (25.7%) | (74.3%) | | |
| t-P | -139.9 | 329.5 | -93.7 | -375.8 | 58.0 | -81.9 |
| | | | (20.0%) | (80.0%) | | |

^aValues in parenthesis give the percentage contribution to the total attractive interactions, $(\Delta E_{elstat} + \Delta E_{orb})$.

In all three cases $\Delta E_{orb} > \Delta E_{elstat}$, hence the nature of $C\equiv C \cdots XC_2H_4$ can be identified as covalent contribution to the chemical bond. Calculated EDA terms reveal that the chemical bonding in Si and Al^- systems is of electron sharing type whereas donor acceptor type in

P^+ system between two fragments. The bond dissociation energy would give an estimate of the relative strength of the $C\equiv C\cdots XC_2H_4$ interaction. Here, we see D_e in tetrahedral structures are larger than those in planar ones in all three isoelectronic systems (Si, Al^- & P^+).

3. Dynamics using classical trajectory calculations

3.1 Analysis of ab initio classical trajectories

The pathways of the stereomutation processes were analyzed by following the internal coordinates θ and ϕ along the ab initio classical trajectories.

[Si(C₄)H₄]

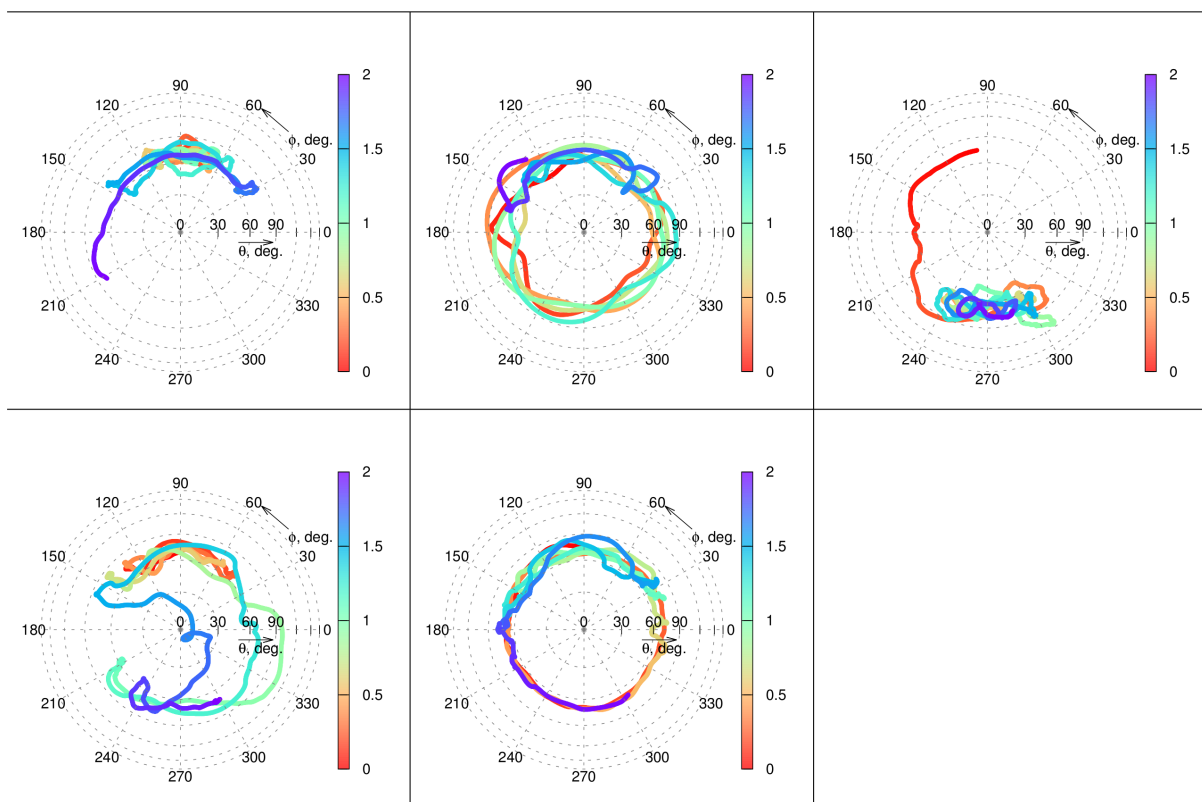
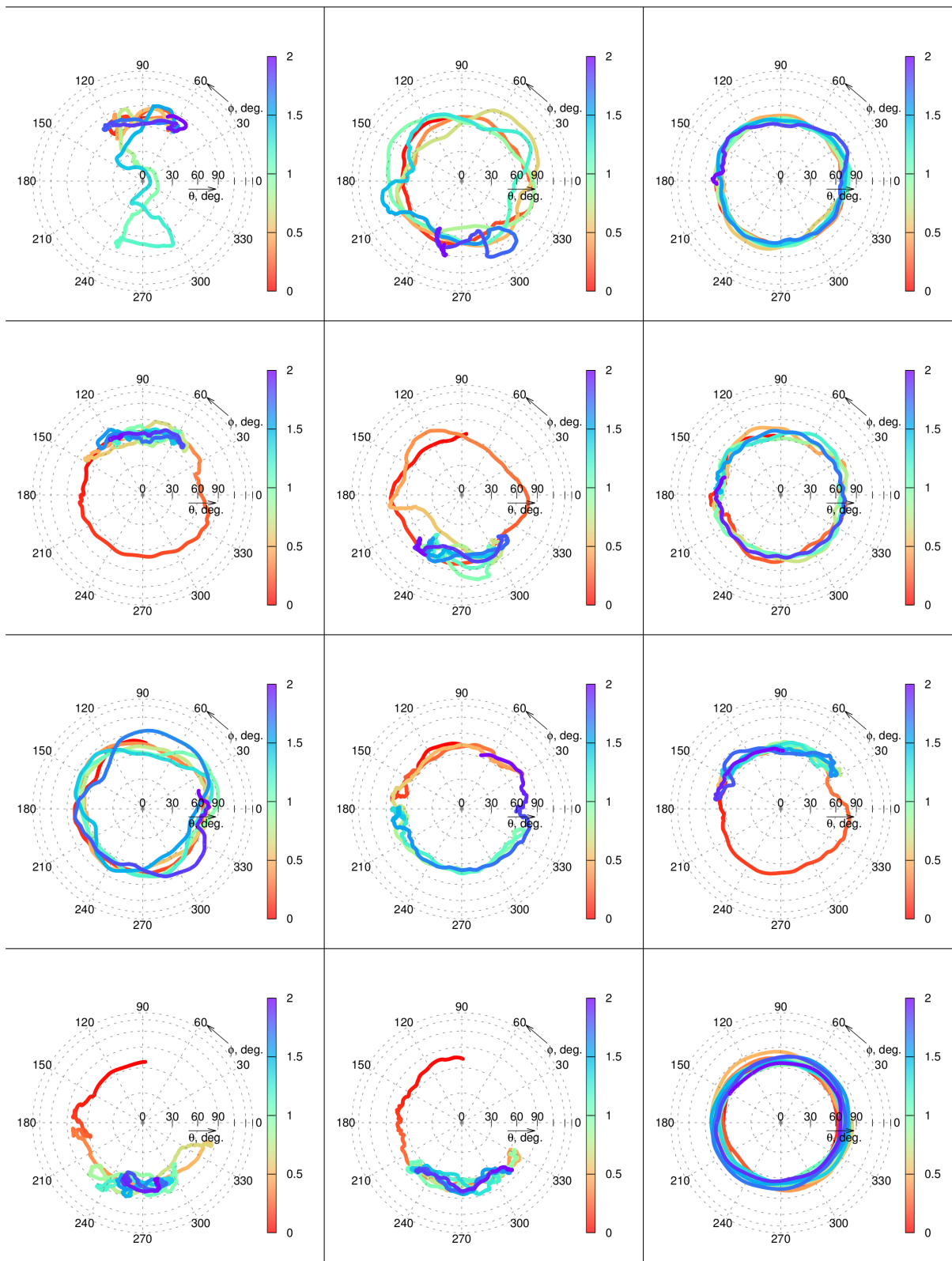
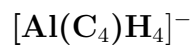
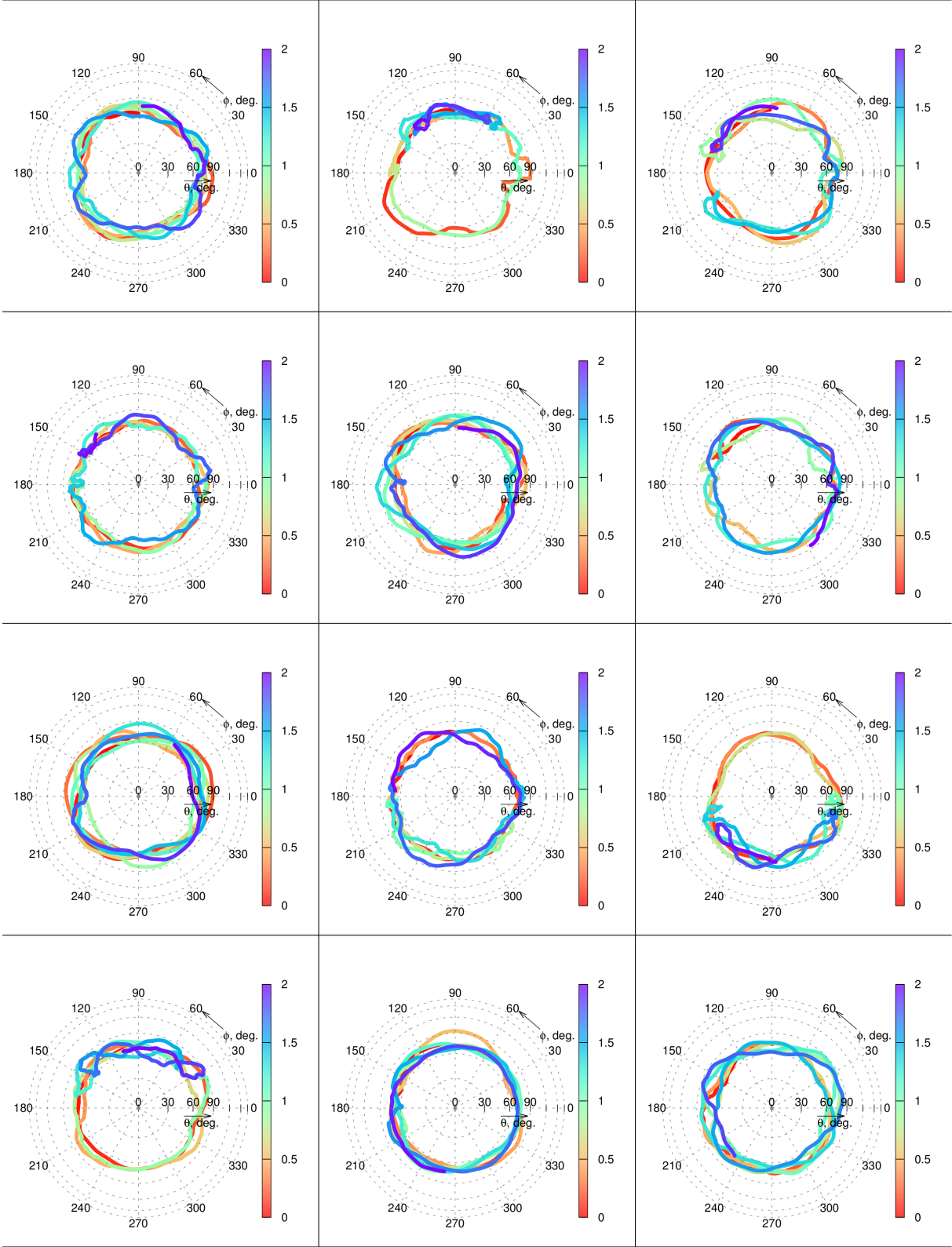


Figure S3: Reactive 5 trajectories for the Si system. Time evolution (2 ps) of internal coordinates: angle between two three-membered rings (ϕ , degree), and $\angle X-C1-C2$ (θ , degree). Color coded as (0→2 ps corresponding red→blue).





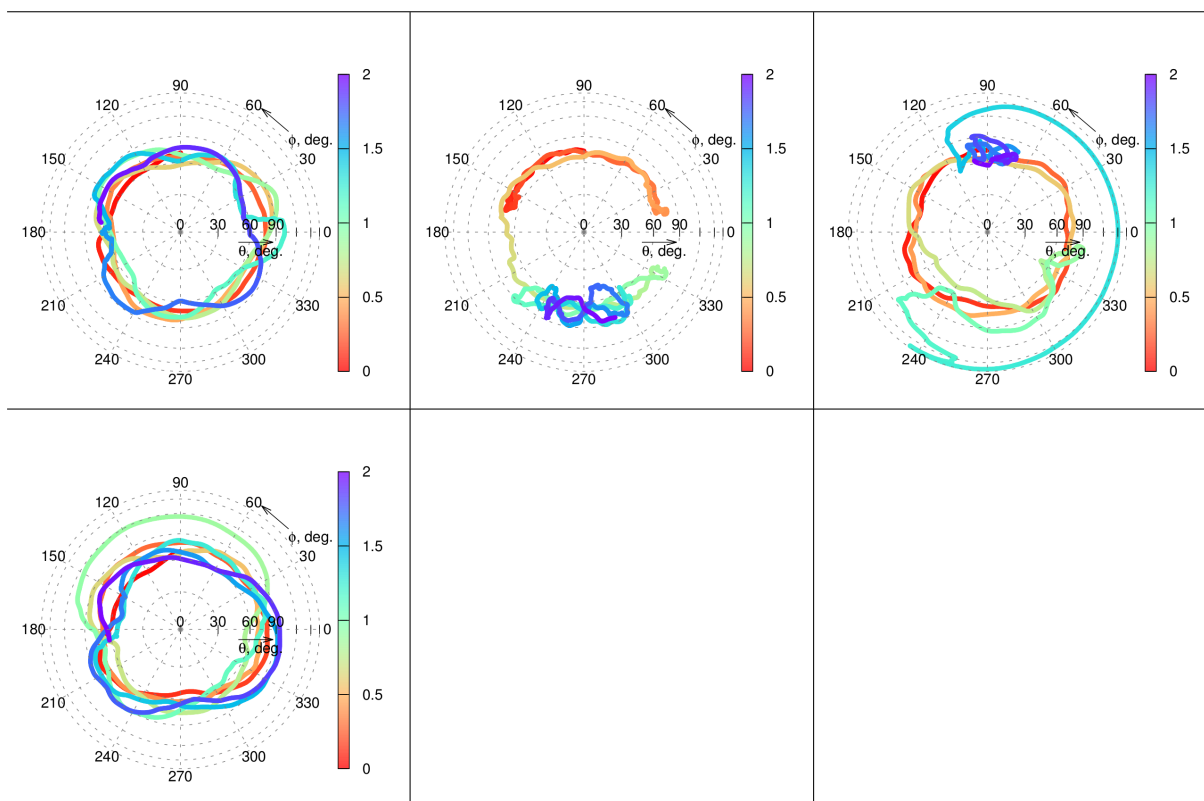
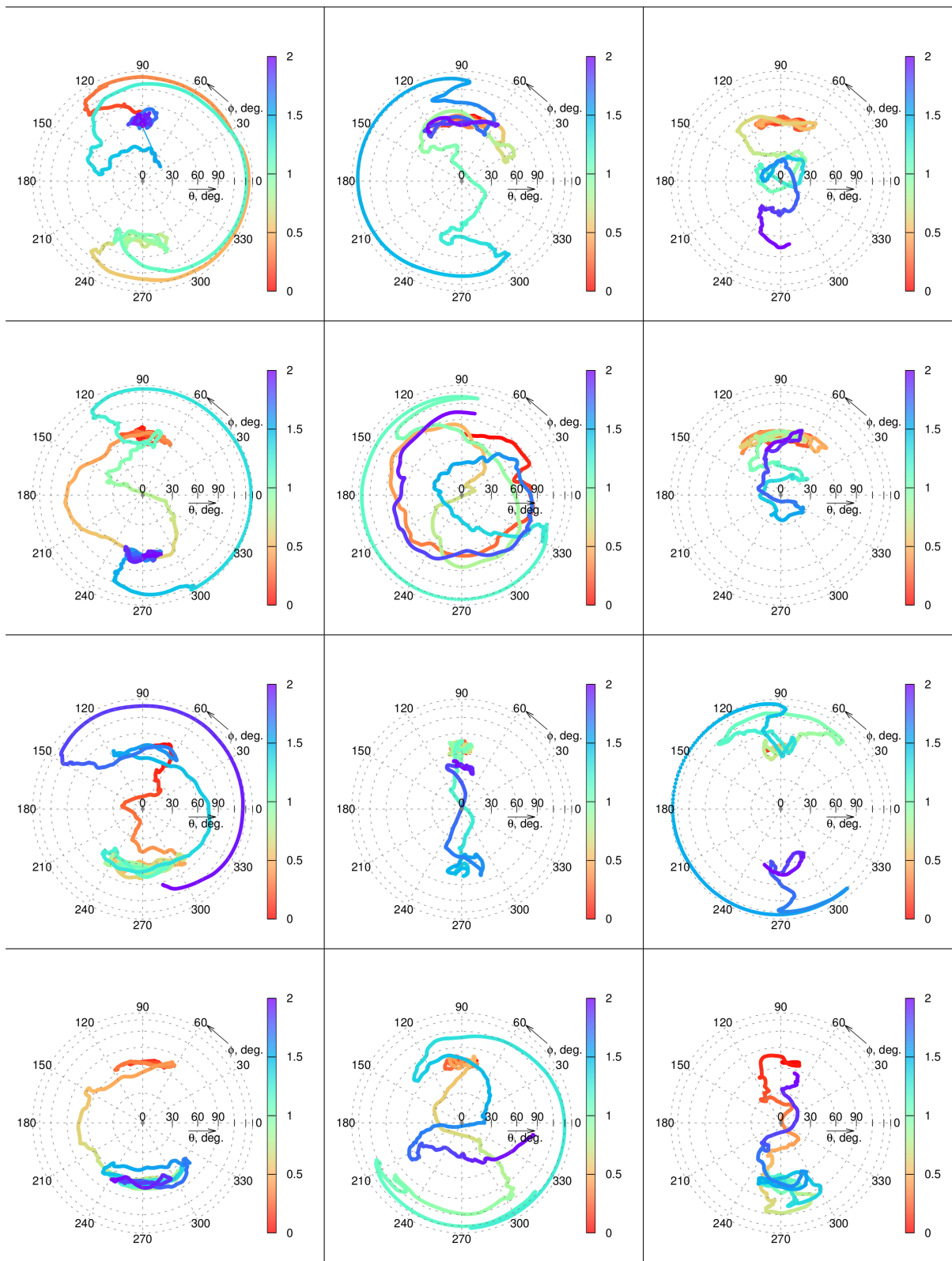
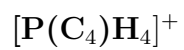
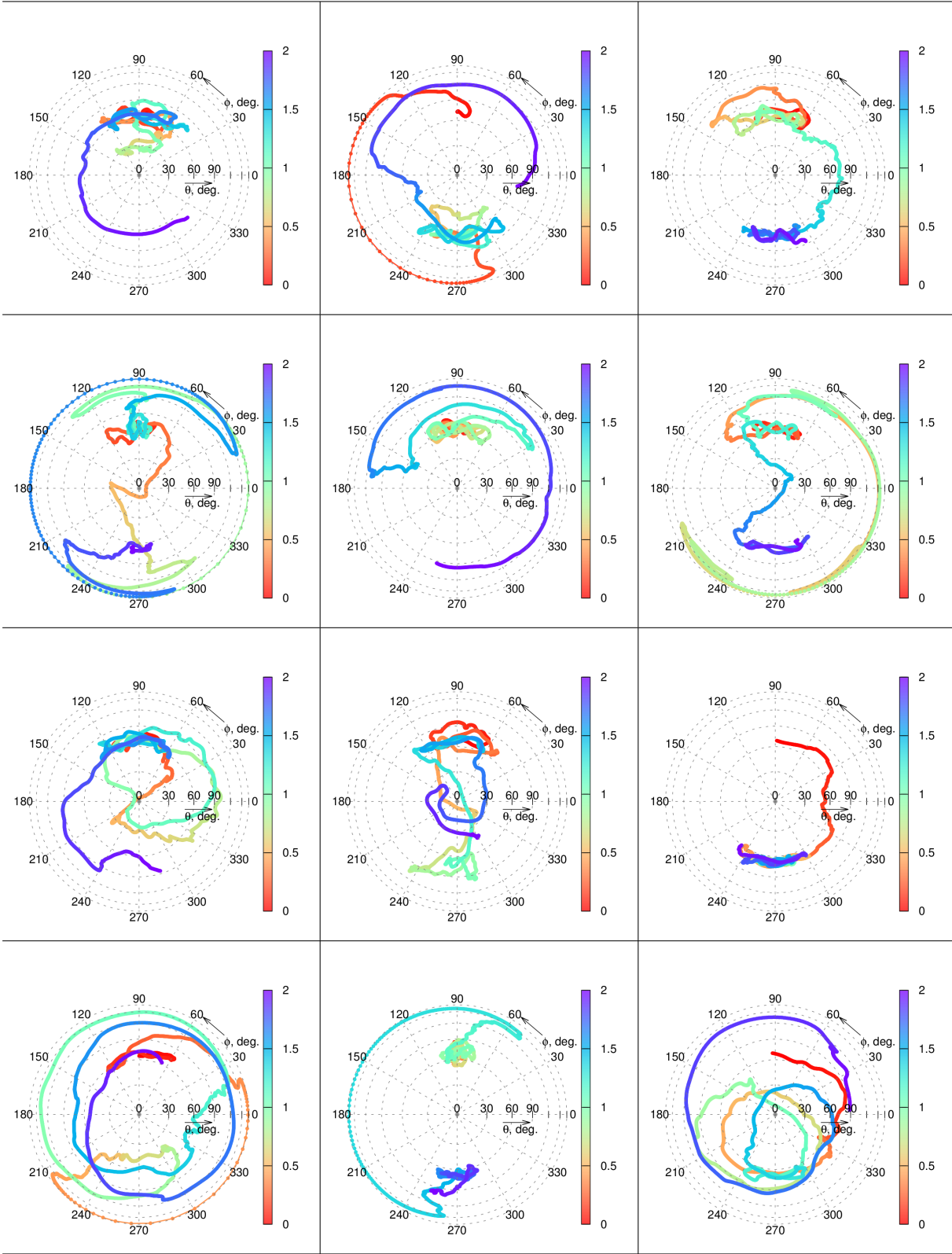


Figure S4: Reactive 28 trajectories for the Al^- system. Time evolution (2 ps) of internal coordinates: angle between two three-membered rings (ϕ , degree), and $\angle\text{X-C1-C2}$ (θ , degree). Color coded as (0→2 ps corresponding red→blue).





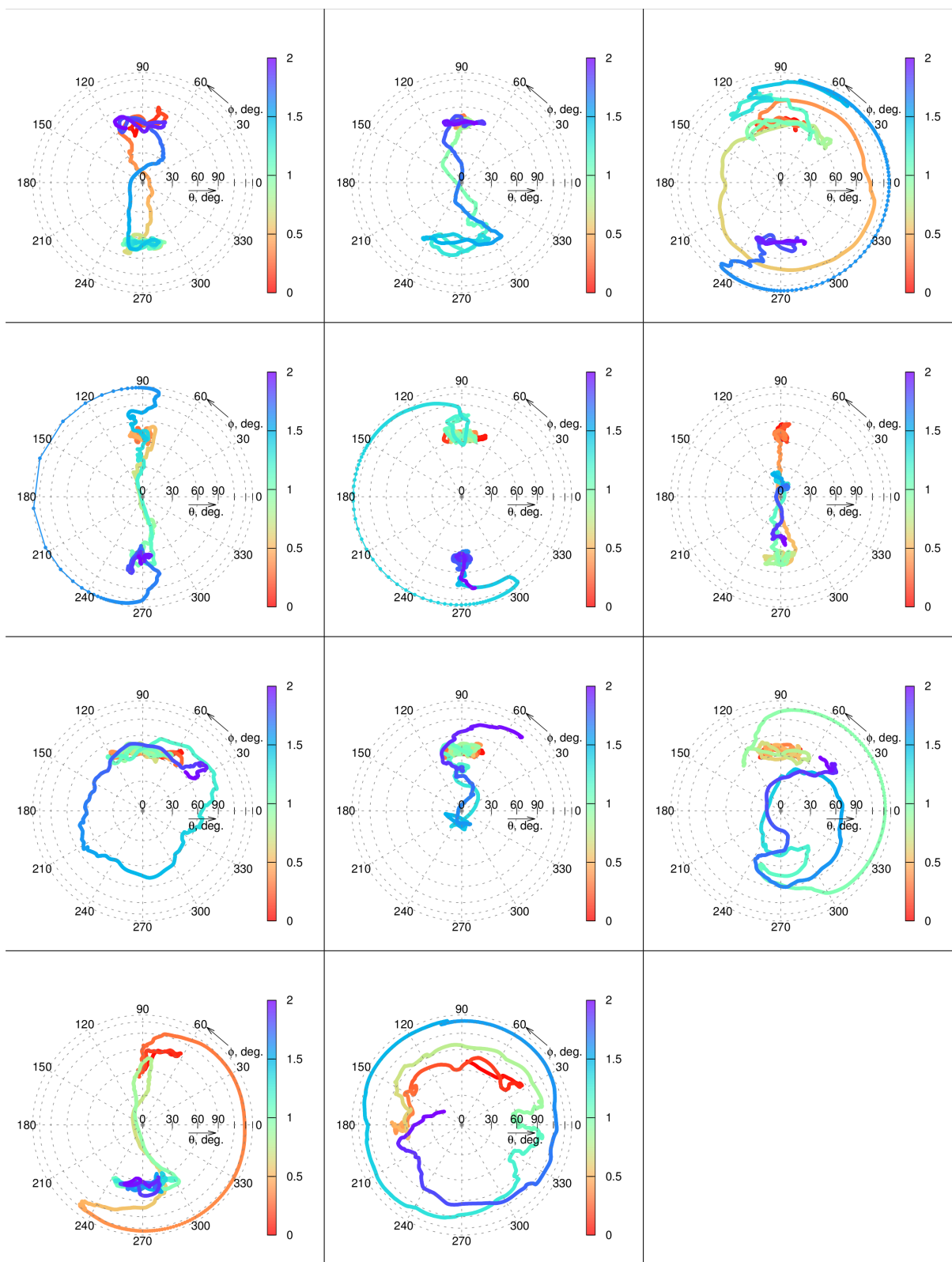


Figure S5: Reactive 35 trajectories for the P^+ system. Time evolution (2 ps) of internal coordinates: angle between two three-membered rings (ϕ , degree), and $\angle X-C1-C2$ (θ , degree). Color coded as (0→2 ps corresponding red→blue).

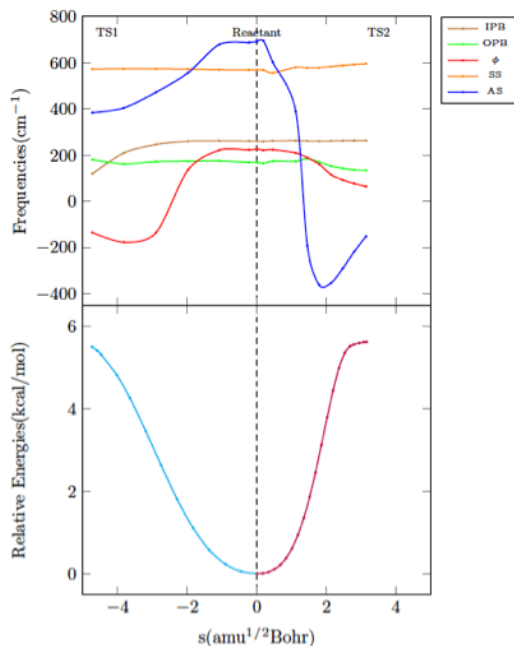


Figure S6: Comparison of harmonic vibrational frequencies along IRC paths for the $[\text{P}(\text{C}_4)\text{H}_4]^+$ molecule. P–C symmetric stretch and asymmetric stretch; torsional and bending vibrations.

The variation of the frequency of the asymmetric P–C stretch along the dissociative reaction path is much larger compared to that of the variation seen for the torsional frequency. In addition, the P–C stretching frequency falls with the range of the torsional frequency in certain region of IRC. Thus the possibility of efficient intramolecular vibrational energy redistribution (IVR) between the asymmetric P–C stretch and the low frequency torsional and bending vibrations along the dissociative reaction path can be seen leading to more trajectories following the dissociative reaction pathway. In the case of the nondissociative isomerization, the coupling between the low frequency and the P–C stretching modes are absent thus facilitating localization of the energies in torsional modes.

Lifetime for isomerization from the trajectories The lifetime from each trajectory undergoing stereomutation were calculated following the angle between the planes (ϕ) and $\angle\text{X-C1-C2}$ (θ) as a function of time. Only the first event of stereomutation was considered in calculating the lifetimes. The transition state structures for stereomutation for $\text{X} = \text{Si}$ and Al^- are planar ($\phi = 0^\circ$). Thus, the lifetime is defined as the time taken by the trajectory

when ϕ changes sign (planar geometry) and θ takes a value between θ_1 and θ_2 . The critical values of θ_1 and θ_2 corresponding to the dissociative transition states are given in Table S6. All the 28 and 5 trajectories undergoing stereomutation for $X = \text{Al}^-$ and Si, respectively did not show any ring opening process prior to the first event of stereomutation. Finally, the lifetimes determined from each trajectory was averaged to obtain the average lifetime of the isomerization process. However, for $X = \text{P}^+$, the transition state structures are non-planar with $\phi = 31.5^\circ$ and -31.5° . The two degenerate transition states are connected via a planar intermediate leading to a double well potential. In this scenario, the stereomutation occurs when the the molecule crosses the second barrier (TS1'), i.e., when $\phi < -31.5^\circ$. Hence the lifetime was calculated when the trajectory crosses the clockwise ($\phi = -31.5^\circ$) or anti-clockwise transition states ($\phi = -148.5^\circ$). It was found that of the 8 trajectories showing stereomutation, 4 were recrossing the TS2 (ring opening transition state) before undergoing stereomutation. Such recrossing trajectories were not taken into account while calculating the average lifetimes. Similar procedure was used for the calculation of lifetimes in the case of $[\text{Si}(\text{C}_2\text{NB})\text{H}_2(\text{CH}_3)_2]$.

Table S6: θ and ϕ parameters used for the calculation of lifetimes for various systems.

| Systems | θ for ring opening TS ($^\circ$) | | ϕ for stereomutation ($^\circ$) | |
|---|---|------------|--|---------------|
| | θ_1 | θ_2 | Clockwise | Anticlockwise |
| $[\text{Si}(\text{C}_4)\text{H}_4]$ | 14.6 | 154.3 | 0.0 | 180.0 |
| $[\text{Al}(\text{C}_4)\text{H}_4]^-$ | 25.2 | 137.8 | 0.0 | 180.0 |
| $[\text{P}(\text{C}_4)\text{H}_4]^+$ | 49.5 | 92.8 | -31.5 | -148.5 |
| $[\text{Si}(\text{C}_2\text{NB})\text{H}_2(\text{CH}_3)_2]$ (Si-B bond breaking) | 17.2 | 148.3 | -23.0 | -164.1 |

Rice-Ramsperger-Kassel-Marcus (RRKM) Lifetimes The RRKM^[6-9] rate constants were computed for all the four model systems using the expression,

$$k(E) = \frac{G(E - E^\ddagger)}{h \rho(E)} \quad (2)$$

where $G(E - E^\ddagger)$ is the sum of states at the transition state region, $\rho(E)$ is the density of states at the minima, E^\ddagger is the barrier for the reaction, and E is the total energy above the classical minima. The rate constants were computed with the total energy used in the trajectory simulation. The density and sum of states were computed by classical counting at a rotational temperature of 0 K. Since for X = Si, Al⁻, and P⁺, the systems are symmetric, so the stereomutation via clockwise and anticlockwise rotation are degenerate and hence a factor of two was used for the reaction path degeneracy.

However, the stereomutation for X= P⁺ and [Si(C₂NB)H₂(CH₃)₂] spiro systems is a two-step process with rate constants k_1 and k_2 : (1) R → Int1 (k_1) and (2) Int1 → R' (k_2); the overall rate constant for these systems is given by the expression $K = k_1/2$.

The lifetimes were then computed from the RRKM rate constant values obtained ($\tau = 1/K$). The lifetimes of all the four systems were found to be in picosecond timescales.

We have also performed a TST rate constant calculation that includes tunnelling coefficient C(T) that uses a one-dimensional Eckart barrier. We found that C(T) was only 1.01, i.e., about 1% at 300 K.

4. Dynamics using BOMD simulations

A continuous part of the BOMD trajectory exhibiting the transitions between **t-Si** and **t*-Si** via either **p-Si** or **p*-Si** transition states is used to make a movie. The traversing of the molecule as observed in the BOMD simulation is captured on the $E(\theta, \phi)$ surface (The two identical carbond atoms C1 and C2 are colored differently for clarity). See attached file (r_to_s_transition.mp4).

4.1 Kinetic analysis by MSM

We have used following geometric criteria for clustering conformations (**t**, **t***, **r** and **r*** four representative states depicted in Figure 2(a), main text) from BOMD simulations of the $\text{Si}(\text{C})_4\text{H}_4$ molecule:

$$\mathbf{t} : r_{\text{Si-C1}} \leq 2.5, r_{\text{Si-C2}} \leq 2.5, 0^\circ \leq \phi \leq 180^\circ$$

$$\mathbf{t}^* : r_{\text{Si-C1}} \leq 2.5, r_{\text{Si-C2}} \leq 2.5, -180^\circ \leq \phi \leq 0^\circ$$

$$\mathbf{r} : r_{\text{Si-C1}} \leq 2.5, r_{\text{Si-C2}} \geq 2.5, -180^\circ \leq \phi \leq 180^\circ$$

$$\mathbf{r}^* : r_{\text{Si-C1}} \geq 2.5, r_{\text{Si-C2}} \leq 2.5, -180^\circ \leq \phi \leq 180^\circ$$

Bond distances are in Å, and ϕ refers to the angle between two three-membered rings of the spiro- $\text{Si}(\text{C})_4$ motif. We have used 661160 number of conformations from a 400 ps long trajectory with the step-size of $0.0242 \times 25 \text{ fs} = 0.605 \text{ fs}$ (0.000605 ps).

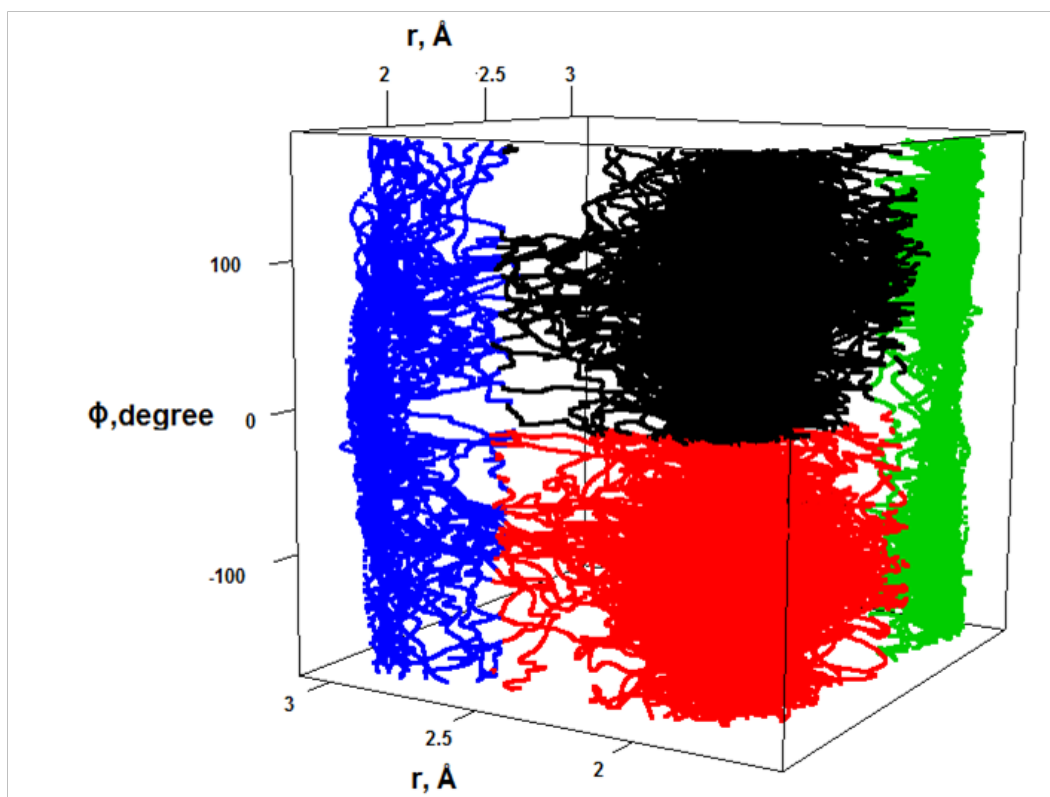


Figure S7: Conformational clustering of four states.

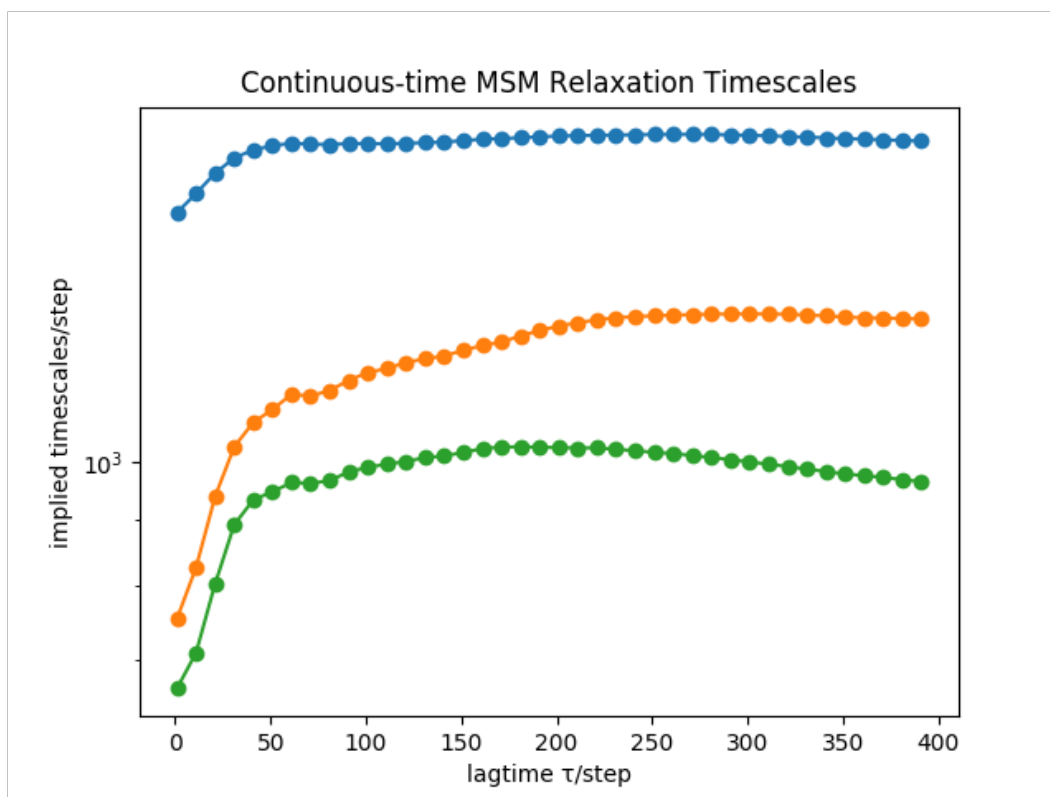


Figure S8: Implied time scale vs. Lag time, step.

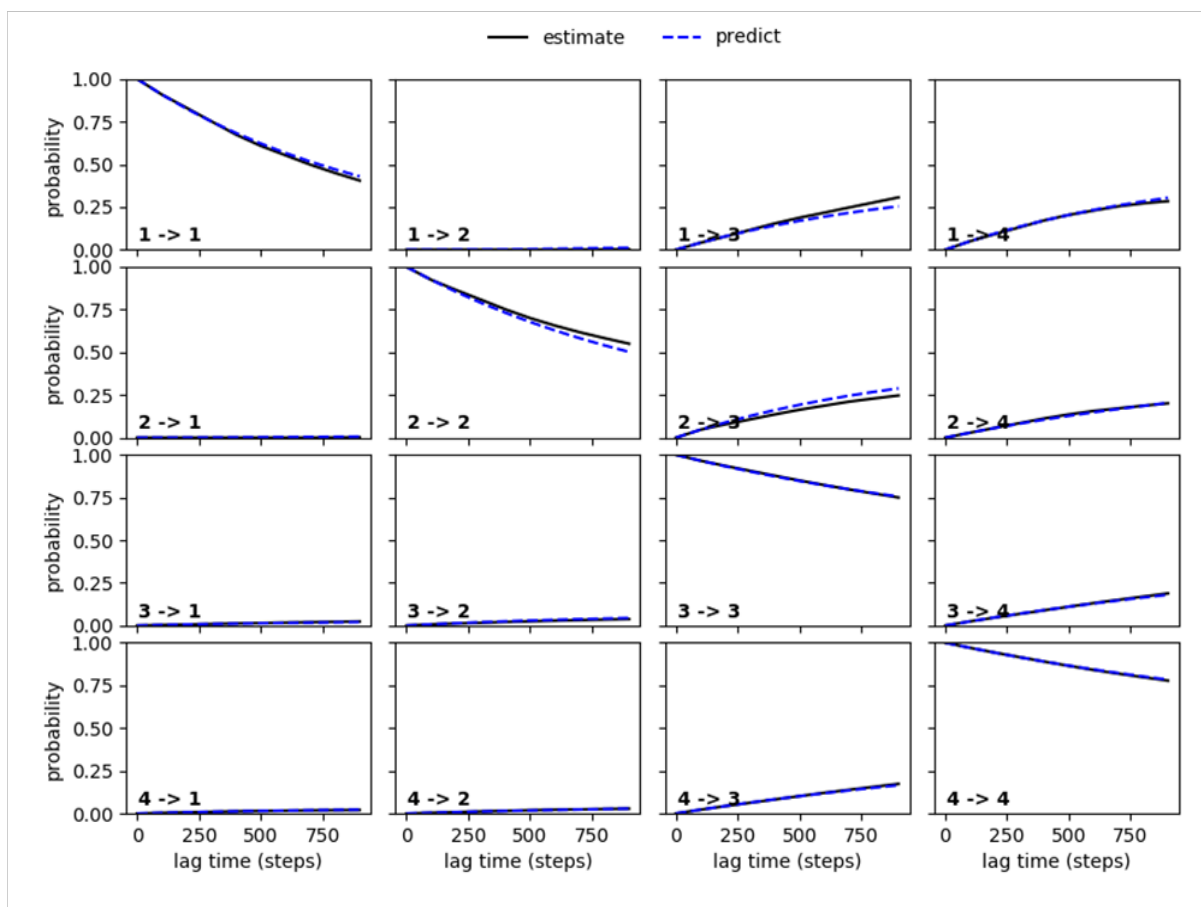


Figure S9: Transition probabilities predicted by the MSM parameterized at lag time $\mathcal{L}=100$ steps (0.06 ps)

4.2 Lifetime of closed and open states

Dwell time distributions $P(t; t_d^*)$ of closed and open states were obtained from a 400 ps long BOMD trajectory of the $\text{Si}(\text{C})_4\text{H}_4$ molecule at $t_d^* = 0.005$ ps. Survival probability distributions $S(t; t_d^*)$ were then calculated using dwell time distributions followed by the best fit to a triexponential function, by which the average lifetimes (Figure 4(c) in main text) of closed and open states were calculated.

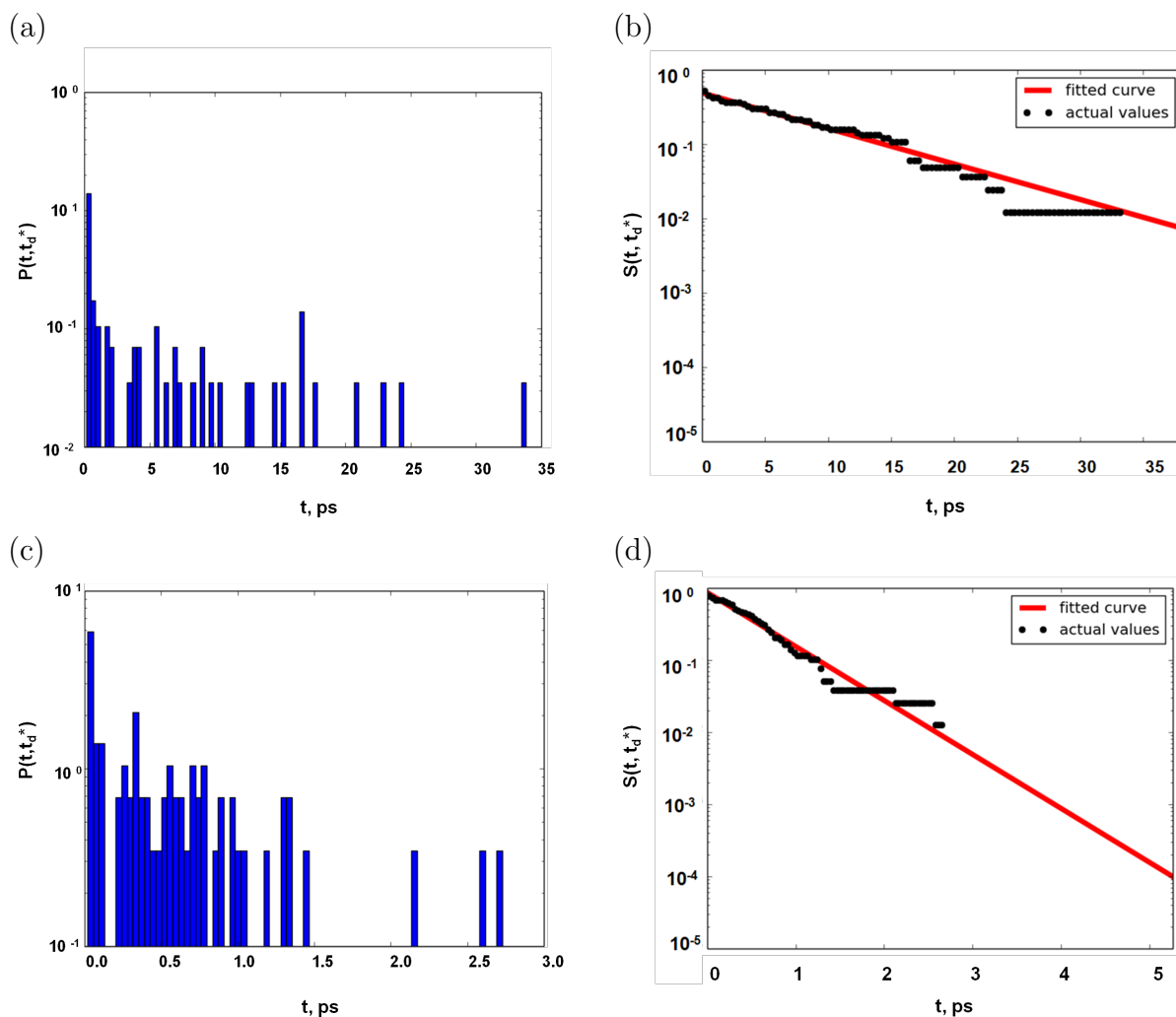


Figure S10: Lifetime calculations of closed (t and t^*) and open (r and r^*) states at $t_d^* = 0.005$ ps. Dwell time distributions $P(t; t_d^*)$ for closed (a) and open (b) states. Survival probability distributions $S(t; t_d^*)$ shown in black dots, and the best fit triexponential function for $S(t; t_d^*)$ indicated by red line for closed (b) and open (c) states.

5. Structures, energies and dynamics of chiral-Si system

In case of the chiral-Si system, structures and energetics were obtained at the MP2/cc-pVTZ level of theory. Ab initio classical trajectories were computed at the MP2/6-31+G(d) level.

| [Si(C ₂ NB)H ₂ (CH ₃) ₂], intermediates | |
|--|---|
| | |
| Z $\theta = 104.9^\circ$ $\phi = 0.0^\circ$ $N_{imag} = 0$ | E $\theta = 96.5^\circ$ $\phi = 180.0^\circ$ $N_{imag} = 0$ |
| | R/S $\theta = 75.3^\circ$ $\phi = 90.0^\circ$ $N_{imag} = 0$ |
| [Si(C ₂ NB)H ₂ (CH ₃) ₂], transition states | |
| | |
| ts1 $\theta = 97.7^\circ$ $\phi = 21.3^\circ$ $N_{imag} = 1(101.9i)$ | ts2 $\theta = 94.8^\circ$ $\phi = 10.1^\circ$ $N_{imag} = 1(53.8i)$ |
| [Si(C ₂ NB)H ₂ (CH ₃) ₂], ring-opened states | |
| | |
| r1 $\theta = 158.6^\circ$ $\phi = 0.0^\circ$ $N_{imag} = 2(66.9i, 32.3i)$ | r2 $\theta^a = 175.5^\circ$ $\phi = 0.0^\circ$ $N_{imag} = 0$ |
| Species | E_{rel} |
| Z | 8.016 |
| E | 6.976 |
| R/S | 0.00 |
| ts1 | 8.124 |
| ts2 | 6.984 |
| r1 | 9.922 |
| r2 | 22.626 |

Figure S11: Optimized structures and selected geometrical parameters of two planar (p1 & p2), tetrahedral (t) minima, and two transition states (ts1 & ts2) of the chiral-Si system at MP2/cc-pVTZ level of theory. Bond distances (in Å), angle between two three-membered rings (ϕ , degree), \angle Si-N-B (θ , degree), and N_{imag} representing number of imaginary frequency with values given in parentheses. Relative energies of transition states/intermediates (in kcal mol⁻¹) at the MP2/cc-pVTZ level of theory for the chiral-Si system. ^a \angle Si-B-N

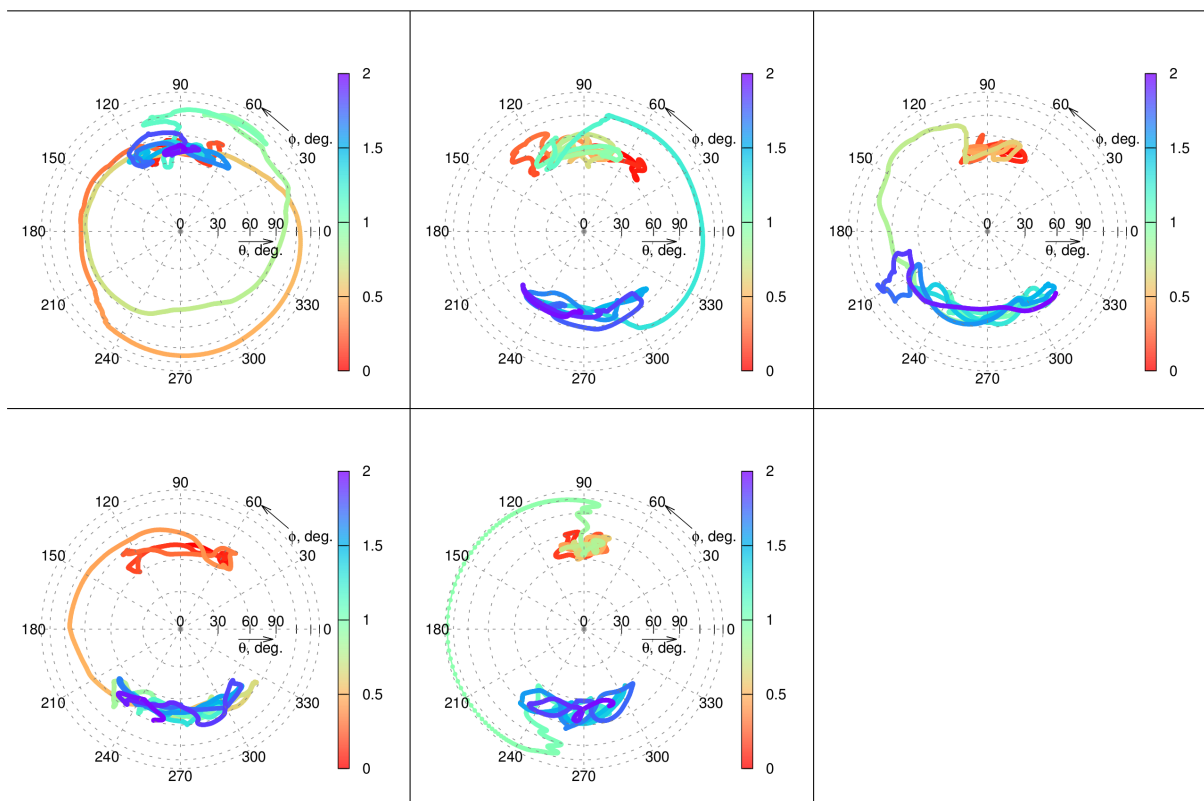


Figure S12: Reactive 5 trajectories for the chiral-Si system. Time evolution (2 ps) of internal coordinates: angle between two three-membered rings (ϕ , degree), and $\angle\text{Si-N-B}$ (θ , degree). Color coded as (0 \rightarrow 2 ps corresponding red \rightarrow blue).

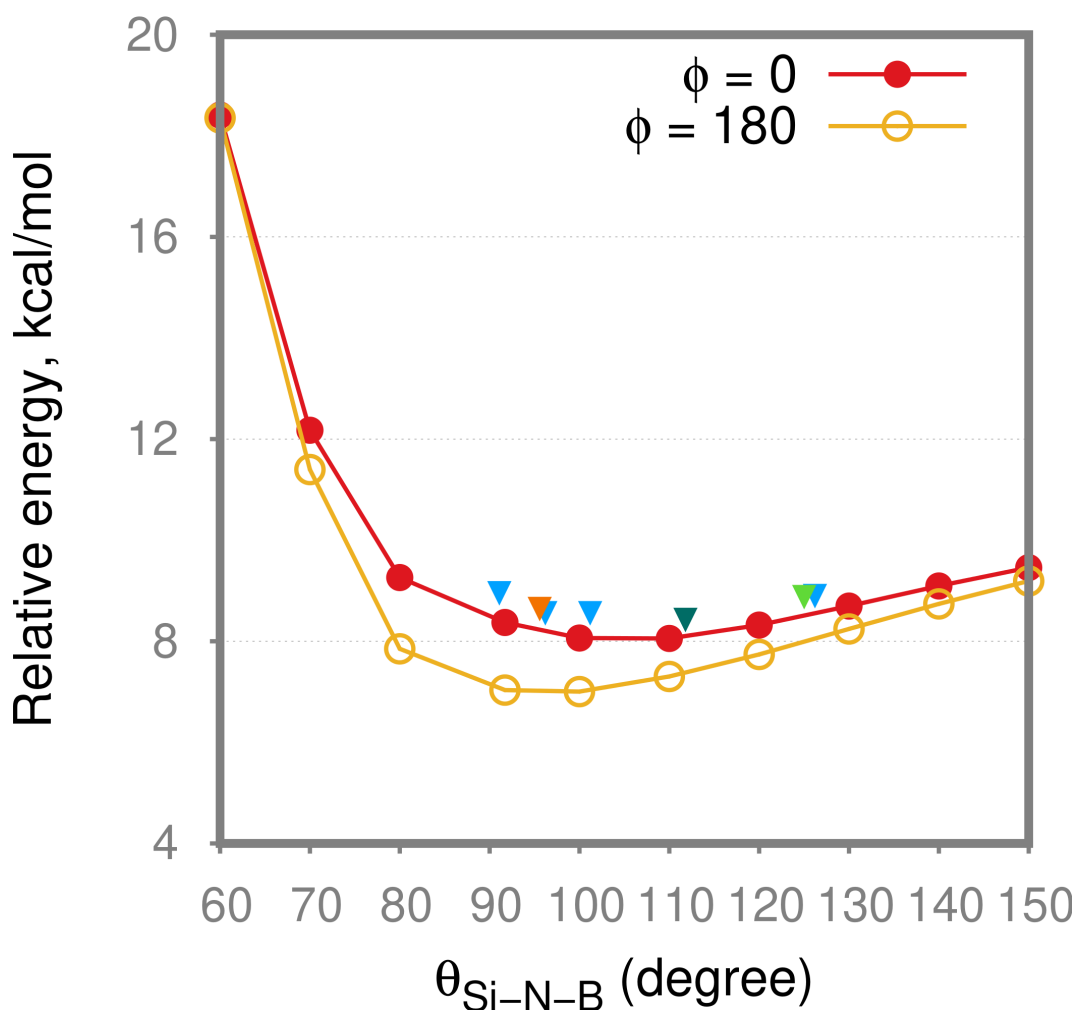


Figure S13: PESs of the (Z) and (E) ($\phi = 0$ and 180 degree respectively) states of the chiral system (in kcal mol⁻¹) with respect to $\angle\text{Si-N-B}$ (θ , degree) obtained at the MP2/cc-pVTZ level of theory. Five reactive trajectories (see Fig. S12), except the last one consist of seven racemization events. The values of θ of the planar states in the trajectory during the process of racemization are marked by inverted triangles. Based on the fact that these points lie in the shallow potential energy minimum as that of the planar state, they were considered to be closed state.

REFERENCES

- (1) Hopffgarten, M. v.; Frenking, G. Energy decomposition analysis. *Wiley Interdisciplinary Reviews: Computational Molecular Science* **2012**, *2*, 43–62.
- (2) Snijders, J.; Vernooijs, P.; Baerends, E. Roothaan-Hartree-Fock-Slater atomic wave functions: single-zeta, double-zeta, and extended Slater-type basis sets for $_{87}\text{Fr}$ - $_{103}\text{Lr}$. *Atomic Data and Nuclear Data Tables* **1981**, *26*, 483–509.
- (3) te Velde, G.; Bickelhaupt, F. M.; Baerends, E. J.; Fonseca Guerra, C.; van Gisbergen, S. J. A.; Snijders, J. G.; Ziegler, T. Chemistry with ADF. *J. Comput. Chem.* **2001**, *22*, 931–967.
- (4) Guerra, C. F.; Snijders, J.; te Velde, G. t.; Baerends, E. Towards an order-N DFT method. *Theor. Chem. Acc.* **1998**, *99*, 391–403.
- (5) Baerends, E. J. et al. ADF2017, SCM, Theoretical Chemistry, Vrije Universiteit, Amsterdam, The Netherlands, <https://www.scm.com>.
- (6) Marcus, R. A.; Rice, O. The kinetics of the recombination of methyl radicals and iodine atoms. *J. Chem. Phys.* **1951**, *55*, 894–908.
- (7) Marcus, R. A. Unimolecular dissociations and free radical recombination reactions. *J. Chem. Phys.* **1952**, *20*, 359–364.
- (8) Rosenstock, H. M.; Wallenstein, M.; Wahrhaftig, A.; Eyring, H. Absolute rate theory for isolated systems and the mass spectra of polyatomic molecules. *Proc. Natl. Acad. Sci. USA* **1952**, *38*, 667.
- (9) Zhu, L.; Hase, W. L. A general RRKM program. QCPE 644, Quantum Chemistry Program Exchange, Indiana University.